DOI: 10.1002/ejic.200901225

Heteroleptic Guanidinate- and Amidinate-Based Complexes of Hafnium as New Precursors for MOCVD of HfO_2

Ke Xu,[a] Andrian P. Milanov,[a] Manuela Winter,[a] Davide Barreca,[b] Alberto Gasparotto,[c] Hans-Werner Becker,[d] and Anjana Devi*[a]

Keywords: Hafnium oxide / Chemical vapor deposition / Thin films / Precursors

The synthesis and characterization of four new heteroleptic complexes $[Hf\{\eta^2\text{-}(i\text{PrN})_2CNMe_2\}_2Cl_2]$ (**1**), $[Hf\{\eta^2\text{-}(i\text{PrN})_2CNMe_2\}_2Me_2]$ (**2**), $[Hf\{\eta^2\text{-}(i\text{PrN})_2CMe\}_2Cl_2]$ (**3**), and $[Hf\{\eta^2\text{-}(i\text{PrN})_2CMe\}_2Me_2]$ (**4**) are reported. All the complexes were characterized by spectroscopic methods, while compounds **1**–**3** were further examined by single-crystal X-ray diffraction, revealing that the complexes are monomers with the hafnium center in a distorted octahedral geometry. The thermal properties of the chlorine-free complexes (**2**, **4**) were examined to determine their suitability for metalorganic chemical vapor deposition (MOCVD) applications, and compound **2** showed good volatility and thermal stability. On the basis of these results, compound **2** was selected for MOCVD of HfO_2 with oxygen as oxidant. Depositions were carried out on Si(100) substrates in the temperature range 300–700 °C. The as-deposited HfO_2 films crystallized in the monoclinic phase at temperatures above 500 °C, and the composition analysis determined by Rutherford back-scattering (RBS) and X-ray photoelectron spectroscopy (XPS) revealed that the films were stoichiometric and free of carbon. Thus, alkylguanidinatohafnium complex **2** is a promising precursor for growing HfO_2 films in a wide temperature range with the desired stoichiometry, because of its adequate volatility, sufficient temperature window between vaporization and decomposition, as well as its ability to decompose cleanly in the presence of oxygen.

Introduction

Thin films of HfO_2 find numerous potential applications ranging from optical fibers, sensors, thermal barrier coatings, waveguides, dielectric layers in complementary metal oxide semiconductor (MOS) devices, etc.[1–5] Among the various methods used to grow thin films, metalorganic chemical vapor deposition (MOCVD) is a preferred technique, as it enables uniform deposition over large areas, conformal coverage on complex device geometries, good composition control, etc. One of the primary requirements for a successful MOCVD process is the availability of appropriate precursors with adequate volatility and stability.[6] There have been several reports in which precursor engineering has been given due importance,[7–12] and the search for better or improved precursors is still in the limelight of research covering metalorganic chemistry. In the case of HfO_2, the conventional metal halides, classical or functional alkoxides, β-diketonates, and alkylamides are the most commonly used precursors.[13–16] However, certain drawbacks such as lower volatility, high evaporation temperatures, limited thermal stability, sensitivity to air and moisture, a high ratio of carbon and nitrogen contamination are associated with these compounds. Some of these issues were addressed in our previous studies, in which we are able to tune the thermal properties of alkoxide- and amide-based precursors for HfO_2 thin film deposition.[17–19] In both cases, we exploited the concept of using chelating ligands in combination with alkoxides or amides in order to saturate the metal center, which results in stable monomeric complexes that are volatile and display improved thermal stability. Metalorganic complexes with amidinates as chelating ligands have been used as precursors for CVD of metal oxide thin films.[20] It has been reported that the related guanidinate ligands offer a similar coordination environment but increased stability due to the possibility of an additional zwitterionic resonance structure.[21] We reported the use of guanidinates as chelating ligands in combination with hafnium alkylamides that resulted in promising precursors for HfO_2.[19] They were successfully utilized for the growth of high quality HfO_2 by using MOCVD[19] and liquid injection metalorganic chemical vapor deposition (LI-MOCVD) techniques.[22]

[a] Inorganic Materials Chemistry, Ruhr-University Bochum, 44801 Bochum, Germany
Fax: +49-234-32-14174
E-mail: anjana.devi@rub.de
[b] CNR-ISTM and INSTM, Department of Chemistry, Padova University, via Marzolo, 1, 35131 Padova, Italy
[c] Department of Chemistry, Padova University and INSTM, via Marzolo, 1, 35131 Padova, Italy
[d] Dynamitron-Tandem-Laboratorium (DTL) of RUBION, Ruhr-University Bochum, 44801 Bochum, Germany
Supporting information for this article is available on the WWW under http://dx.doi.org/10.1002/ejic.200901225.

 © 2010 Wiley-VCH Verlag GmbH & Co. KGaA, Weinheim

In follow up of our recent successful work on precursor engineering, we applied a similar strategy this time for alkyl-based hafnium compounds. Taking amido-guanidinato complexes of Hf as starting point, we adopted two approaches, namely (i) substitution of the amide groups by alkyl groups and (ii) substitution of the guanidinate ligands by amidinate ligands. In this study, the complexes synthesized and characterized were (i) dichloridobis(*N*,*N*′-diisopropyl-2-dimethylamidoguanidinato)hafnium(IV) [Hf{η²-(*i*PrN)₂CNMe₂}₂Cl₂] (**1**), (ii) dimethylbis(*N*,*N*′-diisopropyl-2-dimethylamidoguanidinato)hafnium(IV) [Hf{η²-(*i*PrN)₂-CNMe₂}₂Me₂] (**2**), (iii) dichloridobis(*N*,*N*′-diisopropyl-2-methylamidinato)hafnium(IV) [Hf{η²-(*i*PrN)₂CMe}₂Cl₂] (**3**), and (iv) dimethylbis(*N*,*N*′-diisopropyl-2-methylamidinato)hafnium(IV) [Hf{η²-(*i*PrN)₂ CMe}₂Me₂] (**4**). As our final aim was to evaluate the newly developed compounds for MOCVD applications, only the chlorine-free complexes, **2** and **4**, were considered for investigating the thermal properties to assess the volatility and decomposition behavior essential for thin film deposition. On the basis of these results, compound **2** was found to possess the necessary characteristics for a CVD precursor and was therefore selected for HfO_2 thin film growth with oxygen as oxidant. Herein, we report the details of the synthesis and characterization of complexes **1**–**4** as well as the preliminary results on the MOCVD growth and characterization of HfO_2 thin films with compound **2**.

Results and Discussion

(i) Precursor Synthesis, Spectroscopic and Structural Characterization

In our previous work, different kinds of six-coordinate amido-guanidinato-hafnium(IV) complexes [Hf{η²-(*i*PrN)₂-CNR¹R²}₂(NR¹R²)₂] (R¹ = R² = Me; R¹ = Me, R² = Et; R¹ = R² = Et) were synthesized by insertion reactions of *N*,*N*′-diisopropylcarbodiimide into the Hf–N bonds of tetrakis(dialkylamido)hafnium(IV) complexes [Hf(NR¹R²)₄].[18] The sensitivity of these mixed-amide compounds to air and moisture are significantly reduced relative to the parent alkyl amides, because the coordination sphere of the metal center is saturated. According to thermal analysis, these compounds are volatile, show an adequate temperature window between volatilization and decomposition, and have a constant sublimation rate, meeting all the necessary requirements for a MOCVD process.

In comparison to amide-based Hf precursors, alkyl-based Hf precursors are very volatile, but handling them can be problematic, because they are pyrophoric and highly reactive towards air and moisture.[23] Thus, using chelating ligands such as amidinates and guanidinates in combination with alkyl groups is the strategy employed to modify the chemical properties of alkyl-based Hf precursors. Hf complexes **1**–**4** were synthesized by a salt metathesis route, which is depicted in Scheme 1. The salt metathesis route is chosen for this work, because it offers a broad window in which the guanidinate/amidinate ligands, as well as the alkyl groups, can be varied.

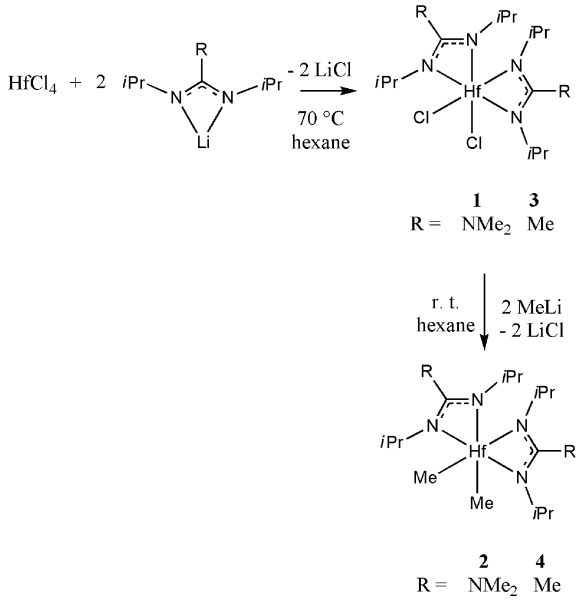

Scheme 1. Synthesis of compounds **1**–**4**.

The lithiated *N*,*N*′-diisopropylguanidinato and *N*,*N*′-diisopropylamidinato ligands used in this work were prepared by the reaction of *N*,*N*′-diisopropylcarbodiimide with $LiNMe_2$ and MeLi, respectively. Since this reaction gives a nearly quantitative yield of lithiated guanidinato and amidinato ligand, a freshly prepared solution of the corresponding lithium guanidinate and amidinate were used directly in the subsequent salt metathesis reactions. The treatment of a hexane slurry of $HfCl_4$ with 2 equiv. of lithiated ligands afforded two new heteroleptic hafnium complexes, **1** and **3**. Compounds **1** and **3** were further treated with 2 equiv. of MeLi, and this resulted in compounds **2** and **4**.

Compounds **1**–**3** were then isolated as white crystalline solids, whereas compound **4** remained as a liquid. The melting points of compounds **1**, **2**, and **3** are 158, 90, and 110 °C, respectively. The spectroscopic and analytical data show that complexes **1**–**4** are monomers. The molecular structures of compounds **1**–**3** in the solid state are shown in Figure 1a–c, and the selected bond lengths and bond angles are listed in Table 1.

Six-coordinate complex **2** (Figure 1b) crystallizes in the triclinic space group ($P\bar{1}$) in a distorted octahedral geometry around the Hf(IV) center with two *cis*-arranged chelating dimethylamidoguanidinate ligands and two methyl groups. The main distortion at the Hf center arises from the bite angles subtended by the guanidinate ligands, which show significant deviation from the 90° angles of a perfect octahedron (60.77° and 60.82°). Similar structural features are also reported for the analogous amidoguanidinatohafnium(IV) complex [Hf{η²(*i*PrN)₂CNMe₂}₂(NMe₂)₂] (58.7° and 58.9°).[18] In contrast to the bite angles of the ligands,

 © 2010 Wiley-VCH Verlag GmbH & Co. KGaA, Weinheim

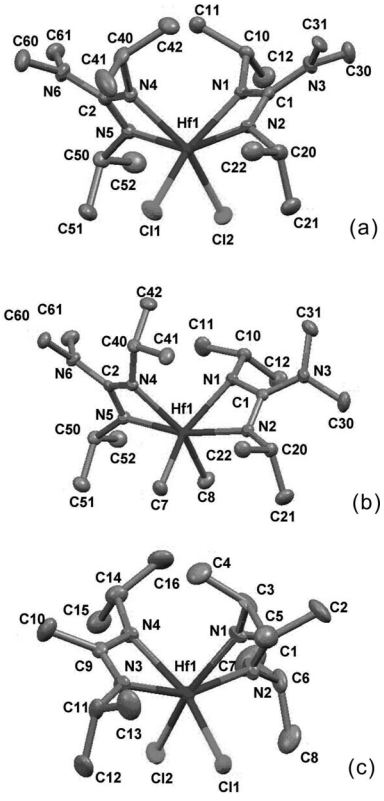

Figure 1. Molecular structures of compounds (a) **1**, (b) **2**, and (c) **3**.

the angles of the two methyl groups with the hafnium atom are nearly ideal 90° angles (92.0°). Because of the weak π-donating effect of the methyl groups, it is expected that the *trans*-effect should not be present in this complex. This expectation was confirmed by comparing Hf–N bond lengths that are similar to each other (Hf1–N1 2.230 Å, Hf1–N2 2.247 Å, Hf1–N4 2.236 Å, and Hf1–N5 2.247 Å). The Hf1–C7 distance (2.261 Å) is slightly longer than that of Hf1–C8 (2.253 Å), and it is almost comparable to Hf–Me distances found in $HfMe_2[C_4H_3N(CH_2NMe_2)_2]_2$ (average: 2.257 Å).[24]

The other two monomeric complexes, **1** (Figure 1a) and **3** (Figure 1c), are also formed as distorted octahedrons according to their molecular structure in the solid state. The bite angles subtended by the guanidinate ligands and amidinate ligands are close to those of complex **2** reported above (60.38° and 60.56° for complex **1** and 61.29° and 60.66° for complex **3**, as compared with 60.77° and 60.82° for complex **2**, respectively). According to the bond lengths in Table 1, the Hf–N bonds of both complexes are about 0.05 Å shorter than those observed for complex **2** (Hf1–N1 2.202 Å and Hf1–N2 2.175 Å for complex **1**; Hf1–N1 2.231 Å and Hf1–N2 2.182 Å for complex **3** relative to Hf1–N1 2.230 Å, Hf1–N2 2.247 Å for complex **2**). This phenomenon could probably be explained by the stronger π-donating character of the chlorine atom in complexes **1** and **3**.

Room-temperature ^{1}H NMR spectra were recorded for compounds **1**–**4**. As expected, compounds **1** and **3** gave three different resonances, and compounds **2** and **4** gave four different resonances. This fact can be clarified by the rapid rotation around the C_2 axis of the molecule as well as the internal C_2 rotation of the ligands in the solvent (Supporting Information), which is faster on the NMR spectroscopic time scale. As a representative example, compound **2** is selected for explaining the symmetries in solution at room temperature. On one side, the two guanidinate ligands are magnetically equivalent as a result of the C_2 symmetry of the molecule in solution, which is consistent with the symmetry observed in the solid state (Figure 1b). On the other side, rotation of the ligand about its internal C_2 axis equilibrates the four isopropyl methyl groups of each guanidinate ligand. This phenomenon is also observed in the case of related guanidinate and amidinate complexes.[25,26]

Additional characterization of compounds **1**–**4** was carried out by using electron impact mass spectrometry (EI-MS, 70 eV). Interestingly, very similar fragmentation patterns with a defined molecular ion peak, M^+, were obtained for compounds **1**–**3**, which indicate that these complexes decomposed following a similar pathway under mass spectrometric conditions. Compound **4**, however, does not show the molecular ion peak or fragments in its mass spectrum. All fragments observed in the EI-MS spectra of compounds **1**–**4** are summarized in Table 2. From the fragmentation pattern of compound **2**, the molecular ion peak (M^+) was detected at m/z = 552. The first four fragmentations observed can be assigned to the stepwise cleavage of four isopropyl groups (m/z = 509, 466, 423, 379). The following two fragments, detected at m/z = 335 and 292, correspond to the subsequent eliminations of two dimethylamide groups. On the basis of the results obtained, a probable fragmenta-

Table 1. Selected bond lengths and bond angles for compounds **1**–**3**.

Compound **1**		Compound **2**		Compound **3**	
Bond lengths (Å)					
Hf1–Cl1	2.422(1)	Hf1–C7	2.261(2)	Hf1–Cl1	2.422(2)
Hf1–Cl2	2.425(1)	Hf1–C8	2.253(2)	Hf1–Cl2	2.413(1)
Hf1–N1	2.202(3)	Hf1–N1	2.230(2)	Hf1–N1	2.231(4)
Hf1–N2	2.175(4)	Hf1–N2	2.247(2)	Hf1–N2	2.182(4)
Bond angles (°)					
Cl1–Hf1–Cl2	92.00(5)	C7–Hf1–C8	91.55(5)	Cl1–Hf1–Cl2	94.38(6)
N1–Hf1–N2	60.38(16)	N1–Hf1–N2	60.77(13)	N1–Hf1–N2	61.29(15)
N4–Hf1–N5	60.56(16)	N4–Hf1–N5	60.82(13)	N4–Hf1–N5	60.66(16)

 © 2010 Wiley-VCH Verlag GmbH & Co. KGaA, Weinheim

Table 2. Overview of the fragments observed in the EI-MS spectra.[a]

Compound	1		2		3		4	
Fragment	Mass *m*/*z*	Rel. int. (%)	Mass *m*/*z*	Rel. int. (%)	Mass *m*/*z*	Rel. int. (%)	Mass *m*/*z*	Rel. int. (%)
M^+	589	21	522	19	531	15	n.d.	n.d.
$M^+ - i$Pr	547	12	509	1	489	33	n.d.	n.d.
$M^+ - 2i$Pr	504	2	466	1	446	1	n.d.	n.d.
$M^+ - 3i$Pr	461	4	423	1	402	1	n.d.	n.d.
$M^+ - 4i$Pr	418	16	379	1	359	1	n.d.	n.d.
$M^+ - 4i$Pr-NMe_2	375	4	335	1	n.d.	n.d.	n.d.	n.d.
$M^+ - 4i$Pr-$2NMe_2$	334	2	292	1	n.d.	n.d.	n.d.	n.d.
L^+	170	35	n.d.	n.d.	n.d.	n.d.	142	26

[a] M^+: molecular ion; L: *i*PrNC(NMe_2)N*i*Pr (for compounds **1** and **2**) or *i*PrNCMeN*i*Pr (for compounds **3** and **4**); n.d.: not detected.

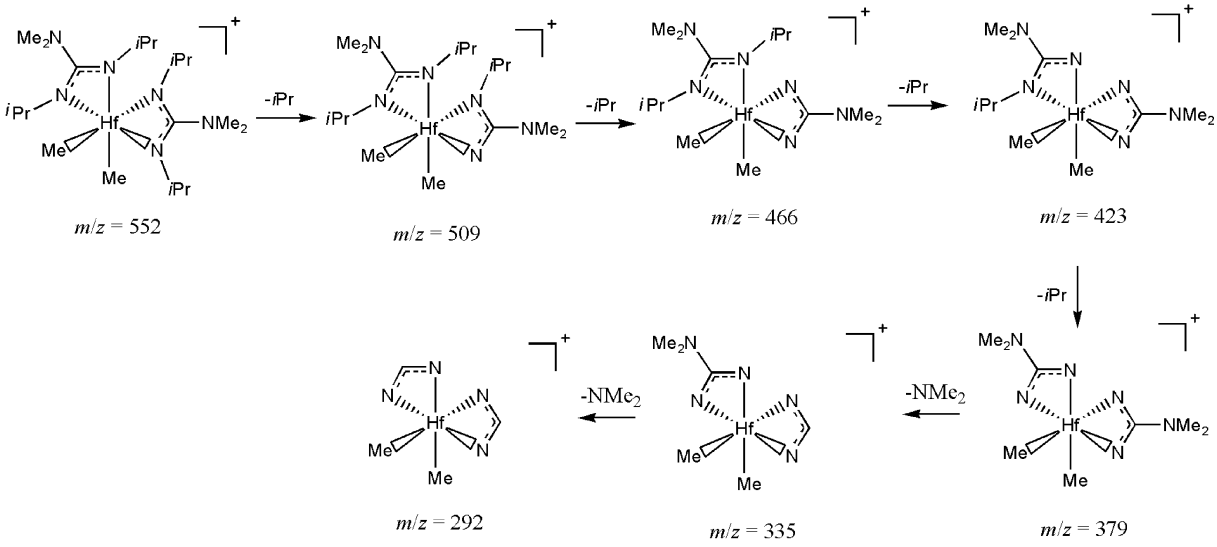

Scheme 2. Proposed fragmentation pattern of compound **1** under mass spectrometric conditions (EI-MS, 70 eV).

tion pattern is proposed in Scheme 2. In contrast to compound **2**, compound **4** shows a fragmentation pattern without the molecular ion peak M^+, which is expected at *m*/*z* = 491. Only one peak at *m*/*z* = 142 could be assigned, which could be assumed to be the methylamidinate ligand.

(ii) Thermal Characterization

In view of the potential application of the synthesized compounds as precursors for MOCVD of HfO_2, their thermal properties were of immediate interest. Our goal was to evaluate the halogen-free precursors for MOCVD applications. In this context, compounds **2** and **4**, which are free of chlorine, were investigated.

The thermal properties of compounds **2** and **4** were studied by thermogravimetric (TG) analysis, and the results are shown in Figure 2. Depending on the chelating ligand used, the TG curves show some pronounced changes in the thermal behavior. The temperature onset of volatilization for compound **2** is much lower than that of compound **4**. At temperatures as low as 50 °C, there is a gradual weight loss observed till about 250 °C followed by a step in the TG curve, which could be attributed to the partial decomposition of compound **2**. At temperatures above 325 °C, a rest mass of 18% is left behind, indicating that the precursor decomposes. In contrast, compound **4** shows a higher onset temperature of volatilization, and also what is more apparent are the multiple steps observed in the TG curve. After the initial weight loss observed at around 150 °C, there is some sign of decomposition taking place as evidenced by a step at 172 °C. When the temperature is further increased, there is an additional weight loss observed, and finally at temperatures above 325 °C a residue of 34% is left behind, indicating that the compound has decomposed. These results imply that the structure of the ligands around the metal center has a certain influence on the thermal properties of the resulting complexes. From the thermal analysis, one can surmise that compound **2** is volatile with an adequate temperature window between volatilization and decomposition, thus showing the desired precursor properties for MOCVD.

During a CVD process, it is important that the precursor possess sufficient thermal stability in order to avoid premature reaction in the gas phase. Thus the thermal stability of compound **2** was additionally evaluated by performing NMR spectroscopic decomposition studies. The compound was sealed in a heavy-walled NMR tube and heated to a desired temperature in an oven periodically for a prolonged

 © 2010 Wiley-VCH Verlag GmbH & Co. KGaA, Weinheim

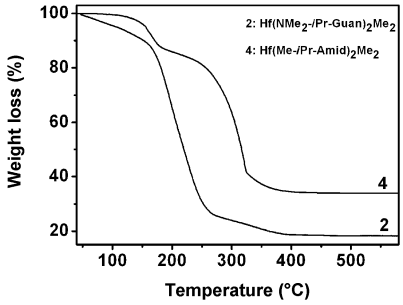

Figure 2. Thermogravimetric analysis curves for Hf complexes **2** and **4**.

period (7 days). ^{1}H NMR spectra were recorded after the tubes were cooled to room temperature. By comparing the integral areas of the NMR peaks, normalized to the solvent peak (C_6D_5H), the amount of undecomposed compound was estimated, and the corresponding half-life of the precursor at the given temperature was determined. Figure 3 shows the temperature-dependent NMR spectroscopic studies carried out at 100 °C for compound **2**. For the freshly prepared samples, only the resonances of this compound can be observed (curve a, resonances 1–3). After the compound was heated at 100 °C for 2 days, some extra peaks appeared, which can probably be attributed to the resonances of *N*,*N*′-diisopropylcarbodiimide (curve b). The intensities of the extra peaks increased after compound **2** was heated for 5 days (curve c), which indicated the increasing amount of carbodiimide. At 100 °C, which is the sublimation temperature of [Hf{η^2-(*i*PrN)$_2$CNMe$_2$}$_2$Me$_2$] (**2**), its half-life is estimated to be 9 days. When the temperature was increased to 140 °C, the half-life was reduced to shorter than 1 day (16 h). The same NMR spectroscopic studies were also performed with a similar compound, [Hf{η^2-(*i*PrN)$_2$CNMe$_2$}$_2$(NMe$_2$)$_2$], in our previous work.[27] This complex shows a remarkable half-life of 18 h at a temperature as high as 220 °C. The exchange of NMe_2 groups with CH_3 leads to a decrease in thermal stability of the corresponding complex, which could probably be explained by the stronger Hf–NMe_2 bond, due to the π-donor character of the amide group. Despite the lower thermal stability of complex **2**, it can still be used as a MOCVD precursor under milder vaporization conditions.

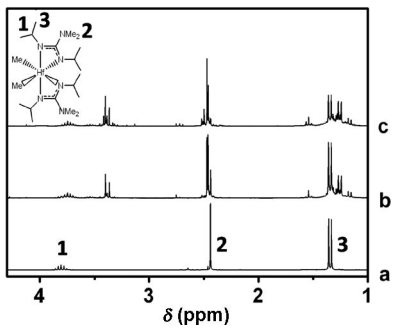

Figure 3. ^{1}H NMR spectra for **2** (a) freshly prepared and (b) kept at 100 °C for 2 days and (c) kept at 100 °C for 5 days.

(iii) HfO_2 Film Growth from Compound 2

The final effort was to illustrate the use of compound **2** as a precursor for MOCVD of HfO_2 thin films. On the basis of the precursor properties evaluated by TG and temperature-dependent NMR spectroscopic studies, complex **2** was identified to be suitable for MOCVD applications as it was found to be more volatile and showed a higher thermal stability relative to compound **4**. Thin film depositions were conducted by using **2** as the precursor together with oxygen as the reactive gas in a cold-wall CVD reactor at temperatures of 300–700 °C. Thin films of HfO_2 were successfully deposited on Si(100) wafers and they were analyzed for their structure, morphology, and composition by using different techniques. The results are discussed below.

(a) Deposition Characteristics

It was possible to achieve HfO_2 film growth at temperatures as low as 300 °C with compound **2**. The films were very uniform and had a shiny appearance. The film thickness was measured by using cross-sectional scanning electron microscopy (SEM), and the growth rates were estimated. Figure 4 shows the Arrhenius plot of HfO_2 growth as a function of substrate temperature. There is an exponential dependence of growth rate in the temperature range 300–500 °C (curve a), which can be assigned to the kinetically controlled regime. At higher temperatures, there is a transformation to the diffusion-dominated region (550–700 °C, curve b), where a nearly constant growth rate was observed. The maximum growth obtained was 7.3 nm/min at 700 °C.

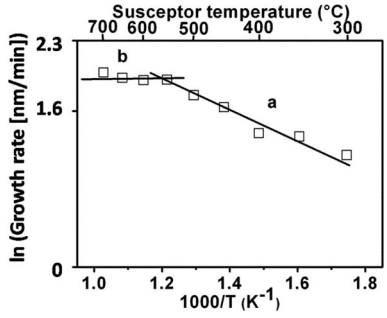

Figure 4. Arrhenius plot of growth rates vs. substrate temperature of HfO_2 films grown from compound **2** on Si(100) substrate.

(b) Film Crystallinity

Figure 5 shows the X-ray diffraction (XRD) pattern of as-deposited HfO_2 films grown at different substrate temperatures. The films at 400 °C were found to be amorphous, and the onset temperature of crystallization was 500 °C, as indicated by the broad (200) reflection corresponding to the monoclinic phase of HfO_2. It should be noted that the temperature onset of crystallization of HfO_2 obtained from compound **2** is about 100 °C lower than that in the previously reported precursor [Hf(NEtMe)$_2$(emaguan)$_2$],[18] which was deposited by using the same MOCVD reactor. This clearly shows that the ligand structure surrounding the

 © 2010 Wiley-VCH Verlag GmbH & Co. KGaA, Weinheim

metal center has a definite influence on the decomposition characteristics of the precursor, which, in turn, affects the film growth characteristics. As the substrate temperature was further raised, the film crystallinity increased, and a small peak for the monoclinic (222) reflection[28] also appeared in addition to the more intense (200) reflection. In addition, at temperatures as high as 600–700 °C, some preferential orientation in the (200) direction was observed.

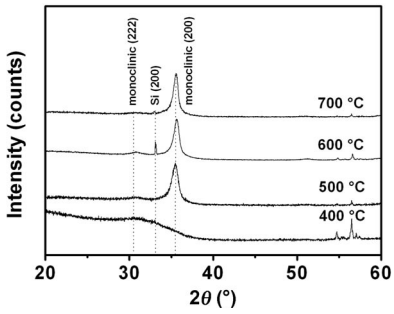

Figure 5. X-ray diffraction patterns of HfO_2 films grown from compound **2** on Si(100) substrates at different substrate temperatures.

(c) Film Morphology

The surface morphology of the as-deposited HfO_2 films was investigated by SEM and atomic force microscopy (AFM). Figure 6 shows the SEM images the HfO_2 films grown at 400 °C and 600 °C (both top and cross-sectional views). The film grown at 400 °C was very dense, which is also confirmed by the cross-sectional SEM micrograph (inset, Figure 6a). It is composed of very small grains that are not fully crystallized, which is in agreement with the results obtained from XRD indicating that the film grown at 400 °C was indeed amorphous. At 600 °C, the film surface seems to be composed of densely packed uniform-sized grains (Figure 6b). The crystallite size was calculated by using the Debye–Scherrer equation, and the average crystallite size is about 12 nm.

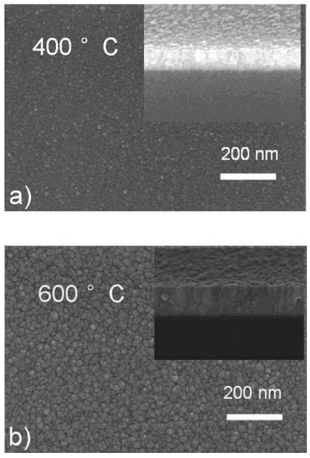

Figure 6. SEM micrographs of HfO_2 films (insets: cross sections) obtained at (a) 400 °C and (b) 600 °C.

The surface roughness of the HfO_2 films was analyzed with AFM, and the result is shown in Figure 7. It was found that the film grown at 400 °C had a surface roughness of 3.0 nm (film thickness = 105 nm), while a slightly higher roughness of 3.9 nm (film thickness 200 nm) was observed for HfO_2 grown at 600 °C. This increased surface roughness can be attributed to the higher crystallinity of the films grown at the higher temperature.

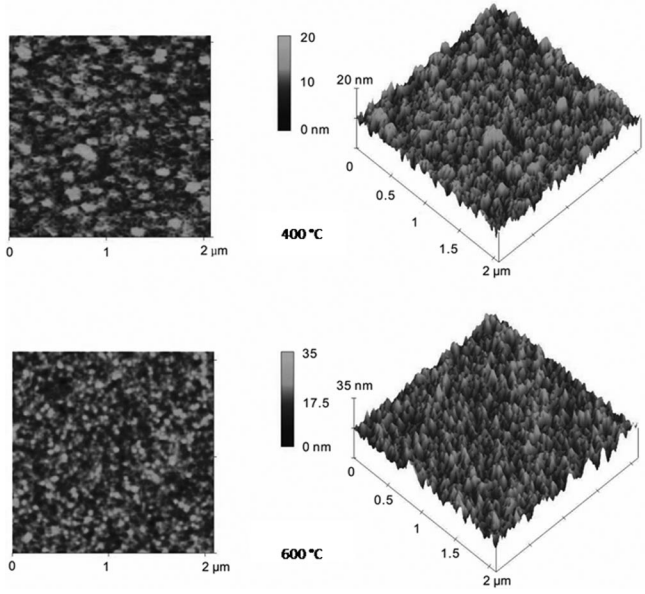

Figure 7. AFM micrographs (plane and 3D views) of HfO_2 films grown from compound **2** on Si(100) at 400 °C (top) and 600 °C (bottom).

(d) Film Composition

In order to investigate the atomic composition of the HfO_2 thin films, energy dispersive X-ray (EDX) and Rutherford back-scattering (RBS) analyses were carried out. The presence of Hf and O in the thin films was confirmed by EDX analysis. The composition of the films grown in the temperature range 300–700 °C was determined by RBS spectroscopy and samples were found to be stoichiometric, with Hf/O ratios varying between 2.1 and 2.3. RBS analysis carried out on a film grown at 500 °C on a Si(100) substrate is depicted in Figure 8. The signals from Hf as well as O in the layer can be seen clearly. The data could be simulated

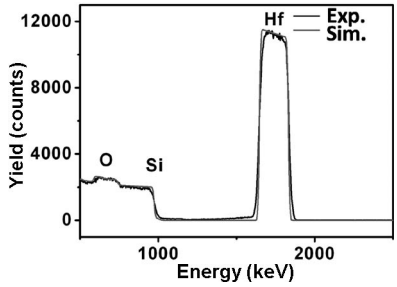

Figure 8. RBS spectrum of an HfO_2 film grown from compound **2** on Si(100) at 500 °C.

 © 2010 Wiley-VCH Verlag GmbH & Co. KGaA, Weinheim

well with the assumption that Hf and O were the only components in the film. No evidence for other elements could be found within experimental error (less than 5%).

X-ray photoelectron spectroscopy (XPS) analyses provided very similar results regarding the chemical composition of the outermost film layers. As an example, Figure 9(a) shows XPS spectra of an HfO_2 film deposited at 500 °C. The wide-scan surface spectrum is characterized by the presence of carbon and oxygen, whose typical atomic percentages are close to 40.0% and 39.0%, respectively. Despite the relatively high carbon content on the surface, it is worth noting that C photoelectron signals were reduced to noise level after Ar^+ erosion [see C1s spectrum (b) in Figure 9], in agreement with RBS results that did not indicate the presence of appreciable amounts of carbon in inner layers of the sample (see above). These observations, along with the absence of nitrogen peaks, suggested a negligible incorporation of precursor residuals in the obtained systems. As a consequence, it could be inferred that the main C source was contact with the outer atmosphere and/or sample manipulation, and that the proposed precursor underwent a clean conversion into HfO_2 under the adopted processing conditions.

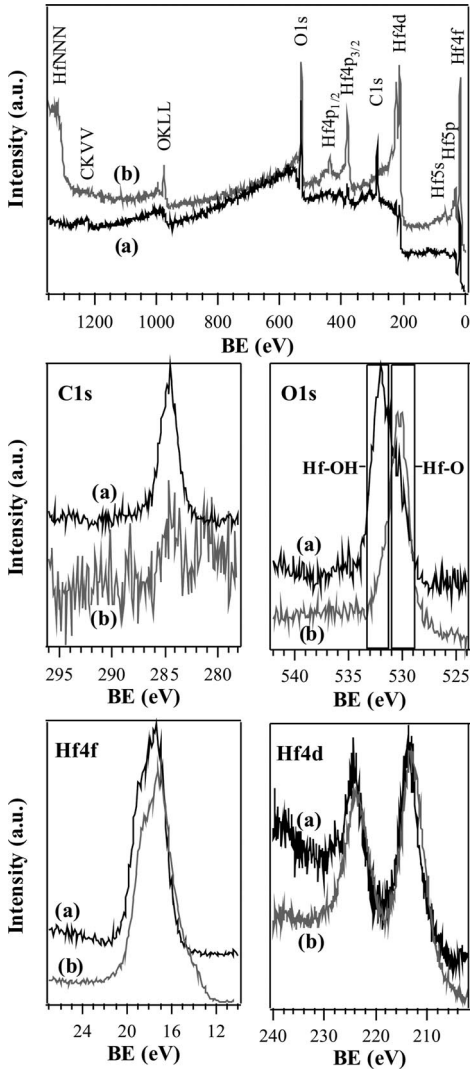

Figure 9. XPS wide-scan spectra and detailed C, O, Hf regions for an HfO_2 thin film grown on Si(100) at 500 °C: (a) surface; (b) after 10 min erosion (Ar^+, 3.5 kV). All spectra are normalized on the *y* scale and vertically shifted for the sake of clarity.

The shapes and positions of hafnium 4f and 4d surface signals [$BE(Hf4f_{7/2})$ = 17.4 eV; $BE(Hf4d_{5/2})$ = 213.6 eV] agreed with the presence of hafnium(IV) oxide,[29–32] in accordance with the above-reported characterization data reported above. Nevertheless, on the sample surface, the O/Hf atomic ratio was 3.8, indicating the presence of an amount of oxygen in excess of that expected for stoichiometric HfO_2 in the outermost regions of the film. A detailed analysis of the surface O1s peak indicated the co-presence of two main contributions centered at BE = 530.3 eV and 531.9 eV. Whereas the former was assigned to lattice oxygen in Hf(IV) oxide, the second one, which was predominant on the sample surface (at least 60% of the total amount of oxygen), could be attributed to surface –OH groups arising from interaction with the outer atmosphere.[30,31] In fact, upon Ar^+ erosion, the O1s band shape underwent an appreciable modification, and the higher BE component was significantly reduced, indicating that hydroxylation phenomena were mostly limited to the surface of the sample. Correspondingly, the O/Hf ratio approached values in the range 1.1–1.2, which are lower than those expected for stoichiometric HfO_2. Beside the removal of surface hydroxy groups, this phenomenon was ascribed to the occurrence of preferential oxygen sputtering,[33] which usually takes place upon ion bombardment of oxide-based materials and was also recently observed by us in the analyses of Nb and Ta oxides.[34] Such a phenomenon, in turn, resulted in an apparent reduction of hafnium, with consequent broadening of the hafnium signals towards the low BE side and, in the case of Hf4f, in the appearance of a low BE tailing.

Summary and Conclusions

Four new mixed dialkylamido-guanidinato and methylamidinato complexes (**1**–**4**) of Hf were synthesized and characterized in detail. In the solid state, the six-coordinate Hf center of complexes **1**–**3** present a distorted octahedral geometry. On the basis of the thermal properties, compound **2** was considered as a suitable precursor for MOCVD. In the temperature range 300–700 °C, HfO_2 thin films were successfully deposited in the presence of oxygen, and it was found that HfO_2 begins to crystallize around 500 °C. The films were smoother at lower temperature because of their amorphous nature. The increase in the roughness of the thin films at higher temperatures can be correlated to crystalline grain growth. The films were found to be stoichiometric and free of any impurities, as determined by RBS and XPS analysis. On the basis of these results, our current effort focuses on testing this precursor for atomic layer deposition (ALD) applications and also evaluating the compatibility of this compound with other precursors (Ti, Zr, Gd, etc.) for the growth of mixed metal oxides by LI-MOCVD.

 © 2010 Wiley-VCH Verlag GmbH & Co. KGaA, Weinheim

Experimental Section

General Procedures: All reactions and manipulations of the compounds were performed in a conventional vacuum/argon line by using standard Schlenk techniques. Starting compounds $HfCl_4$ (Alfa Aesar), *N*,*N*′-diisopropylcarbodiimide (Acros), MeLi (Aldrich), and Me_2NLi (Aldrich) were used as received. Lithium *N*,*N*′-diisopropyl-2-dimethylamidoguanidinato ligands [Li(*i*PrN)$_2$CNMe$_2$] and lithium *N*,*N*′-diisopropyl-2-methylamidinato ligands [Li(*i*PrN)$_2$CMe] were synthesized by following modified literature procedures.[35,36] Samples for analytical characterization were prepared in an argon-filled glove box (MBraun). The solvents employed were dried and purified by an automatic solvent purification system attached directly to the glove box (MBraun solvent purification system). The NMR solvents were degassed and dried with activated molecular sieves. Elemental analyses were performed by using a CHNSO Vario EL instrument. Melting point measurements were carried out in sealed capillaries under Ar. ^{1}H and ^{13}C NMR spectra were recorded with a Bruker Avance DPX 250 spectrometer. NMR spectroscopic decomposition experiments were performed by using heavy-walled NMR tubes, which were heated in an oven for 7 days, and the ^{1}H NMR spectra were recorded periodically with a Bruker Avance DPX 250 spectrometer. Electron impact (EI) mass spectra were recorded with a Varian MAT spectrometer at an ionizing energy of 70 eV. Thermogravimetric analyses (TGA) were performed by using a Seiko TG/DTA 6300S11 instrument (sample weight: ca. 10 mg) at a heating rate of 5 °C/min. All measurements were performed at atmospheric pressure in the temperature range from room temp. to 600 °C under flowing N_2 (99.9999%; flow rate = 300 mL/min).

[Hf{η^2-(*i*PrN)$_2$CNMe$_2$}$_2$Cl$_2$] (1): To a solution of *N*,*N*′-diisopropylcarbodiimide (6.24 mL, 40 mmol) in hexane (50 mL) was added lithium dimethylamide (2.04 g, 40 mmol) in hexane (50 mL) dropwise over a period of 1 h at 0 °C. The resulting solution was stirred overnight and then added to $HfCl_4$ (6.41 g, 40 mmol) dissolved in hexane (50 mL). The yellowish solution was refluxed at 70 °C overnight, and the insoluble byproduct was removed from the solution by filtration. The solution was then concentrated under reduced pressure and kept at 0 °C, which resulted in colorless crystals of **1**. Yield: 4.7 g (40% based on $HfCl_4$). Melting point: 158 °C. $C_{18}H_{40}Cl_2HfN_6$ (589.95): calcd. C 36.92, H 6.84, N 14.36; found C 36.03, H 6.47, N 14.73. ^{1}H NMR (250 MHz, C_6D_6, room temp.): δ = 3.73 [sept., J = 6.5 Hz, 4 H, NC*H*(CH$_3$)$_2$], 2.33 [s, 12 H, (C*H*$_3$)$_2$N], 1.43 [d, J = 6.5 Hz, 24 H, NCH(C*H*$_3$)$_2$] ppm. ^{13}C NMR (250 MHz, C_6D_6, room temp.): δ = 172 {N*C*[NCH(CH$_3$)$_2$]$_2$}, 47 {[(*C*H$_3$)$_2$N]}, 40 {NC[N*C*H(CH$_3$)$_2$]$_2$}, 25 {NC[NCH(*C*H$_3$)$_2$]$_2$} ppm. EI-MS (70 eV): m/z (%) = 589 (21.4) [M]$^+$, 547 (12.2) [M – *i*Pr]$^+$, 504 (2.4) [M – 2*i*Pr]$^+$, 461 (4.0) [M – 3*i*Pr]$^+$, 418 (16.1) [M – 4*i*Pr]$^+$, 375 (4.4) [M – 4*i*Pr – NMe$_2$]$^+$, 334 (2.8) [M – 4*i*Pr – 2NMe$_2$]$^+$, 170 (34.7) [L]$^+$.

[Hf{η^2-(*i*PrN)$_2$CNMe$_2$}$_2$Me$_2$] (2): To a solution of [Hf{η^2-(*i*PrN)$_2$CNMe$_2$}$_2$Cl$_2$] (**1**) (1.69 g, 3 mmol) in hexane (20 mL) was added MeLi (about 3.75 mL, 6 mmol, 1.6 M in Et$_2$O) at 0 °C. The insoluble lithium chloride was removed from the solution by filtration after 24 h of stirring. The solvent was concentrated under reduced pressure and kept at 0 °C overnight. Colorless crystals of **2** were obtained. Yield: 3.1 g (85% based on compound **1**). Melting point: 90 °C. $C_{20}H_{46}HfN_6$ (549.11): calcd. C 43.63, H 7.65, N 15.27; found C 42.65, H 9.52, N 13.50. ^{1}H NMR (250 MHz, C_6D_6, room temp.): δ = 3.81 [sept., J = 6.5 Hz, 4 H, NC*H*(CH$_3$)$_2$], 2.43 [s, 12 H, (C*H*$_3$)$_2$N], 1.35 [d, J = 6.5 Hz, 24 H, NCH(C*H*$_3$)$_2$], 0.68 [s, 6 H, Hf(C*H*$_3$)$_2$] ppm. ^{13}C NMR (250 MHz, C_6D_6, room temp.): δ = 173 {N*C*[NCH(CH$_3$)$_2$]$_2$}, 48 {[Hf(*C*H$_3$)$_2$]}, 47 {[(*C*H$_3$)$_2$N]}, 40 {NC[N*C*H(CH$_3$)$_2$]$_2$}, 25 {NC[NCH(*C*H$_3$)$_2$]$_2$} ppm. EI-MS (70 eV): m/z (%) = 552 (19.0) [M]$^+$, 509 (1.2) [M – *i*Pr]$^+$, 466 (1.1) [M – 2*i*Pr]$^+$, 423 (1.3) [M – 3*i*Pr]$^+$, 379 (1.4) [M – 4*i*Pr]$^+$, 335 (1.6) [M – 4*i*Pr – NMe$_2$]$^+$, 292 (1.3) [M – 4*i*Pr – 2NMe$_2$]$^+$.

[Hf{η^2-(*i*PrN)$_2$CMe}$_2$Cl$_2$] (3): *N*,*N*′-diisopropylcarbodiimide (25 mL, 40 mmol) diluted in hexane (50 mL) was added to MeLi (25 mL, 40 mmol, 1.6 M in Et$_2$O) at 0 °C. The resulting solution was stirred overnight and added to hafnium chloride (6.41 g, 40 mmol) in hexane (50 mL). The yellowish solution was refluxed at 70 °C overnight, and the insoluble lithium chloride was removed from the solution by filtration. The solution was concentrated and kept at 0 °C. Colorless needles of **3** were obtained after 24 h. Yield: 5.84 g (55% based on $HfCl_4$). Melting point: 110 °C. $C_{16}H_{34}Cl_2HfN_4$ (531.87): calcd. C 36.16, H 6.40, N 10.55; found C 36.18, H 6.39, N 10.64. ^{1}H NMR (250 MHz, C_6D_6, room temp.): δ = 3.49 [sept., J = 6.5 Hz, 4 H, NC*H*(CH$_3$)$_2$], 1.38 [s, 12 H, (C*H*$_3$)$_2$N], 1.28 [d, J = 6.5 Hz, 24 H, NCH(C*H*$_3$)$_2$] ppm. ^{13}C NMR (250 MHz, C_6D_6, room temp.): δ = 178 {N*C*[NCH(CH$_3$)$_2$]$_2$}, 48 [(*C*H$_3$)$_2$N], 25 {NC[N*C*H(CH$_3$)$_2$]$_2$}, 11 {NC[NCH(*C*H$_3$)$_2$]$_2$} ppm. EI-MS (70 eV): m/z = 531 (15.3) [M]$^+$, 489 (32.6) [M$^+$ – *i*Pr]$^+$, 446 (1.2) [M – 2*i*Pr]$^+$, 402 (1.3) [M – 3*i*Pr]$^+$, 359 (1.3) [M – 4*i*Pr]$^+$.

[Hf{η^2-(*i*PrN)$_2$CMe}$_2$Me$_2$] (4): MeLi (5 mL, 8 mmol, 1.6 M in Et$_2$O) was added to [Hf{η^2-(*i*PrN)$_2$CMe}$_2$Cl$_2$] (**3**) (2.13 g, 4 mmol) diluted in hexane (20 mL) at 0 °C. The resulting solution was stirred overnight, and the insoluble lithium chloride was removed from the solution by filtration. The solvent was subsequently extracted under reduced pressure, and **4** was obtained as a yellowish liquid. Yield: 1.6 g (75% based on compound **3**). $C_{18}H_{40}HfN_4$ (491.03): calcd. C 43.99, H 8.15, N 11.41; found C 43.65, H 8.52, N 11.50. ^{1}H NMR (250 MHz, C_6D_6, room temp.): δ = 3.59 [sept., J = 6.4 Hz, 4 H, NC*H*(CH$_3$)$_2$], 1.50 [s, 12 H, (C*H*$_3$)$_2$N], 1.23 [d, J = 6.5 Hz, 24 H, NCH(C*H*$_3$)$_2$], 0.57 [s, 6 H, Hf(C*H*$_3$)$_2$] ppm. ^{13}C NMR (250 MHz, C_6D_6, room temp.): δ = 177 {N*C*[NCH(CH$_3$)$_2$]$_2$}, 49 {[(*C*H$_3$)$_2$N]}, 48 {[Hf(*C*H$_3$)$_2$]}, 25 {NC[N*C*H(CH$_3$)$_2$]$_2$}, 11 {NC[NCH(CH$_3$)$_2$]$_2$} ppm.

X-ray Structure Determination: Single crystals of compounds **1**, **2**, and **3** mounted on thin glass capillaries were cooled to the data collection temperature (150 K) on an X-Calibur 2 Oxford diffractometer with graphite monochromated Mo-K_α radiation (λ = 0.71073 Å). The structure was solved by using the *SHELXL-97*[37] software package and refined by full-matrix least-squares methods based on F^2 with all observed reflections. A summary of the data collection and crystallographic parameters is given in Table 3. CCDC-756068 (for **1**), -756069 (for **2**), and -756070 (for **3**) contain the supplementary crystallographic data for this paper. These data can be obtained free of charge from The Cambridge Crystallographic Data Centre via www.ccdc.cam.ac.uk/data_request/cif.

Thin Film Deposition: A horizontal cold-wall MOCVD reactor[38] operated under reduced pressure was employed for film deposition with compound [Hf{η^2-(*i*PrN)$_2$CNMe$_2$}$_2$Me$_2$] (**2**) as the precursor. Films were grown on ultrasonically cleaned Si(100) substrates (SIMAT) without removing the native oxide layer. Nitrogen (flow rate: 50 sccm, 99.9999%) and oxygen (flow rate: 50 sccm, 99.9999%) were used as the carrier and reactive gases, respectively. For each deposition, approximately 100 mg of the precursor was filled into a glass bubbler in a glove box. Depositions were carried out in the substrate temperature range 300–700 °C, while the precursor vaporizer was maintained at 100 °C. Depositions were carried out for 30 min, and the reactor pressure was maintained at 1 mbar.

Film Characterization: The film crystallinity was investigated by XRD analysis by using a Bruker D8 Advance AXS Diffractometer [Cu-K_α radiation (1.5418 Å)] equipped with a position sensitive de-

 © 2010 Wiley-VCH Verlag GmbH & Co. KGaA, Weinheim

Table 3. Crystal data and details of structure determination for compounds **1**–**3**.

	1	**2**	**3**
Formula	$C_{18}Cl_2H_{40}N_6Hf$	$C_{20}H_{46}N_6Hf$	$C_{16}Cl_2H_{34}N_4Hf$
M_r (g/mol)	589.95	549.12	1063.72
Temperature (K)	113(2)	113(2)	111(2)
Wavelength (Å)	0.71073	0.71073	0.71073
Crystal system	monoclinic	triclinic	orthorhombic
Space group	$P2_1/n$	$P\bar{1}$	$Pbca$
a (Å)	9.1095(3)	8.6328(3)	15.7928(16)
b (Å)	16.8261(7)	8.9475(5)	15.9116(7)
c (Å)	16.7565(8)	18.2475(10)	35.7021(16)
α (°)	90	95.508(4)	90
β (°)	104.657(4)	94.559(4)	90
γ (°)	90	115.543	90
Volume (Å^3)	2484.81(18)	1254.35(11)	8971.5(11)
Z	4	2	8
D_{calc} (g/cm^3)	1.577	1.454	1.575
μ (mm^{-1})	4.428	4.174	4.894
F (000)	1184	560	4224
Crystal size (mm)	$0.38 \times 0.20 \times 0.13$	$0.34 \times 0.31 \times 0.28$	$0.28 \times 0.25 \times 0.20$
θ range (°)	2.61–27.58	2.94–25.00	2.82–27.58
Reflections collected	46608	20431	87205
Unique reflections	5722	4407	10352
Completeness to θ (θ = 25)	99.7%	99.6%	99.5%
Data/restraints/parameters	5722/0/244	4407/0/258	10352/0/435
Final R indices [$I > 2\sigma(I)$]	$R1$ = 0.0208; $wR2$ = 0.0574	$R1$ = 0.0135; $wR2$ = 0.0312	$R1$ = 0.0356; $wR2$ = 0.0553
R indices (all data)	$R1$ = 0.0346; $wR2$ = 0.0883	$R1$ = 0.0166; $wR2$ = 0.0318	$R1$ = 0.1020; $wR2$ = 0.0655
Largest diff. peak and hole (e/Å^3)	1.760/–1.596	1.226/–0.614	4.415/–1.025

tector (PSD). All films were analyzed in the θ-2θ geometry. The film thickness and surface morphology were analyzed by SEM with a LEO Gemini SEM 1530 electron microscope. An Oxford ISIS EDX system coupled with the SEM instrument was used for the EDX analysis. XPS spectra were recorded by means of a Perkin–Elmer Φ5600ci spectrometer by using a monochromatized Al-K_α excitation source ($h\nu$ = 1486.6 eV). The binding energy (BE) shifts were corrected by assigning to the C1s line of adventitious carbon a value of 284.8 eV. The estimated standard deviation for BEs was ±0.2 eV. Quantitative analyses were performed according to a previously described procedure.[32] AFM was used in the contact mode for studying the surface roughness with Nanoscope Multimode III AFM. RBS measurements to determine film composition were carried out with a 2-MeV He beam of the Dynamitron-Tandem accelerator in Bochum with beam intensities of about 10 nA. A silicon surface barrier detector with an energy resolution of 15 keV was placed at an angle of 170° with respect to the beam axis. The spectra were analyzed with the program RBX[39] by using the stopping powers of the program SRIM.[40]

Supporting Information (see footnote on the first page of this article): Rotation behavior of compound **2** in the NMR spectroscopic experiments (Figure S1).

Acknowledgments

The authors acknowledge the financial support from the Deutsche Forschungsgemeinschaft (DE-790/9–1) and Prof. R. A. Fischer for his continuous support. K. X. thanks Tatjana Ladnorg for the AFM measurements and the Research School of RUB for financial support.

[1] M. Sayer, K. Sreenivas, *Science* **1990**, *247*, 1056–1060.
[2] G. D. Wilk, R. M. Wallace, J. M. Anthony, *J. Appl. Phys.* **2000**, *87*, 484–492.
[3] K. S. Murphy, *Brit. UK Pat. Appl.* GB 2383339, **2003**.
[4] R. R. Goncalves, G. Carturan, M. Montagna, M. Rerrari, L. Zampddri, S. Pelli, G. C. Righini, S. J. L. Ribeiro, Y. Messaddeq, *Optical Mater.* **2004**, *25*, 131–139.
[5] M. Balog, M. Schieber, M. Michman, S. Patai, *Thin Solid Films* **1977**, *41*, 247–259.
[6] R. A. Fischer, H. Parala in *Chemical Vapor Deposition: Precursors, Processes and Applications* (Eds.: A. C. Jones, M. L. Hitchman), RSC, Cambridge, UK, **2009**, ch. 9.
[7] G. G. Condorelli, G. Malandrino, I. Fragala, *Coord. Chem. Rev.* **2007**, *251*, 1931–1950.
[8] F. T. Edelmann, *Chem. Soc. Rev.* **2009**, *38*, 2253–2268.
[9] J. M. Decams, L. G. Hubert-Pfalzgraf, J. Vaissermann, *Polyhedron* **1999**, *18*, 2885–2890.
[10] R. Pothiraja, A. Milanov, H. Parala, M. Winter, R. A. Fischer, A. Devi, *Dalton Trans.* **2009**, *4*, 654–663.
[11] R. Pothiraja, A. P. Milanov, D. Barreca, A. Gasparotto, H.-W. Becker, M. Winter, R. A. Fischer, A. Devi, *Chem. Commun.* **2009**, 1978–1980.
[12] A. Milanov, R. Thomas, M. Hellwig, K. Merz, H.-W. Becker, P. Ehrhart, R. A. Fischer, R. Waser, A. Devi, *Surf. Coat. Technol.* **2007**, *201*, 9109–9116.
[13] R. C. Smith, T. Ma, N. Hoilien, L. Y. Tsung, M. J. Bevan, L. Colombo, J. Roberts, S. A. Campbell, W. Gladfelter, *Adv. Mater. Opt. Electron.* **2000**, *10*, 105–114.
[14] M. Pulver, G. Wahl, *Proc. Electrochem. Soc.* **1997**, *97–25*, 960–967.
[15] S. Pakswer, P. Skoug in *Thin Dielectric Oxide Films Made by Oxygen Assisted Pyrolysis of Alkoxides* (Eds: J. M. Blocher, J. C. Withers), The Electrochemical Society, Los Angeles, CA, **1970**, p. 619.
[16] A. Bastiani, G. A. Battiston, R. Gerbasi, M. Porchia, S. Daolio, *J. Phys. IV* **1995**, *5*, C-525.
[17] A. Milanov, R. Bhakta, R. Thomas, P. Ehrhart, M. Winter, R. Waser, A. Devi, *J. Mater. Chem.* **2006**, *16*, 437–440.
[18] A. Baunemann, R. Thomas, R. Becker, M. Winter, R. A. Fischer, P. Ehrhart, R. Waser, A. Devi, *Chem. Commun.* **2004**, 1610–1611.

 © 2010 Wiley-VCH Verlag GmbH & Co. KGaA, Weinheim

[19] A. Milanov, R. Bhakta, A. Baunemann, H. W. Becker, R. Thomas, P. Ehrhart, M. Winter, A. Devi, *Inorg. Chem.* **2006**, *45*, 11008–11018.
[20] P. J. Bailey, S. Pace, *Coord. Chem. Rev.* **2001**, *214*, 91–141.
[21] S. J. Coles, M. B. Hursthouse, *Organometallics* **1995**, *14*, 2456–2462.
[22] R. Thomas, E. Rije, P. Ehrhart, A. P. Milanov, R. Bhakta, A. Bauneman, A. Devi, R. A. Fischer, R. Waser, *J. Electrochem. Soc.* **2007**, *154*, G77–G84.
[23] R. K. Thomason, B. O. Patrick, L. L. Scharfer, *Can. J. Chem.* **2005**, *83*, 1037–1042.
[24] K.-C. Hsieh, J.-C. Chang, M.-T. Lee, C.-H. Hu, C.-H. Hung, H. M. Lee, J.-H. Huang, M.-H. Wang, T.-Y. Lee, *Inorg. Chim. Acta* **2004**, *357*, 3517–3524.
[25] S. M. Mullins, A. P. Duncan, R. G. Bergman, J. Arnold, *Inorg. Chem.* **2001**, *40*, 6952–6953.
[26] L. A. Koterwas, J. C. Fettinger, L. R. Sita, *Organometallics* **1999**, *18*, 4183–4190.
[27] K. Xu, A. P. Milanov, A. Devi, *ECS Trans.* **2009**, *25*, 625–632.
[28] JCPDS number: 00-034-0104.
[29] D. D. Sarma, C. N. R. Rao, *J. Electron Spectrosc. Relat. Phenom.* **1980**, *20*, 25–45.
[30] J. F. Moulder, W. F. Stickle, P. E. Sobol, K. D. Bomben, *Handbook of X-ray Photoelectron Spectroscopy*, Perkin–Elmer, Eden Prairie, MN, **1992**.
[31] G. Carta, N. El Habra, G. Rossetto, G. Torzo, L. Crociani, M. Natali, P. Zanella, G. Cavinato, V. Matterello, V. Rigato, S. Kaciulis, A. Mezzi, *Chem. Vap. Deposition* **2007**, *13*, 626–632.
[32] D. Barreca, A. Milanov, R. Fischer, A. Devi, E. Tondello, *Surf. Sci. Spectra* **2007**, *14*, 34–40.
[33] D. Briggs, M. P. Seah, *Practical Surface Analysis: Auger and X-ray Photoelectron Spectroscopy*, Wiley, New York, **1990**.
[34] M. Hellwig, A. Milanov, D. Barreca, J.-L. Deborde, R. Thomas, M. Winter, U. Kunze, R. A. Fischer, A. Devi, *Chem. Mater.* **2007**, *19*, 6077–6087.
[35] D. C. Bradley, I. M. Thomas, *J. Chem. Soc.* **1960**, 3857–3861.
[36] S. L. Aeilts, M. P. Coles, D. C. Swenson, R. F. Jordan, V. G. J. Young, *Organometallics* **1998**, *17*, 3265–3270.
[37] G. M. Sheldrick, *SHELXL-97*, *Program for the Refinement of Crystal Structures*, University of Göttingen, Germany, **1997**.
[38] A. Devi, W. Rogge, A. Wohlfart, F. Hipler, H. W. Becker, R. A. Fischer, *Chem. Vap. Deposition* **2000**, *6*, 245–252.
[39] E. Kótai, *Nucl. Instrum. Methods* **1994**, *B85*, 588–596.
[40] J. F. Ziegler, M. D. Ziegler, J. P. Biersack, SRIM-2008, v. 2008.03;http://www.srim.org.

Received: December 18, 2009
Published Online: March 9, 2010

 © 2010 Wiley-VCH Verlag GmbH & Co. KGaA, Weinheim